Thermoreversible gels – optimisation of processing parameters in fused deposition modelling

Vadodaria, Saumil Sudhir; Warner, Eleanor; Norton, Ian; Mills, Tom B.

DOI:
10.1016/j.colsurfa.2021.126399

Document Version
Peer reviewed version

Citation for published version (Harvard):
Vadodaria, SS, Warner, E, Norton, I & Mills, TB 2021, 'Thermoreversible gels – optimisation of processing parameters in fused deposition modelling', *Colloids and Surfaces A: Physicochemical and Engineering Aspects*, vol. 618, 126399. https://doi.org/10.1016/j.colsurfa.2021.126399

Thermoreversible Gels – Optimisation of Processing Parameters in Fused Deposition Modelling

Saumil Sudhir Vadodaria*[1], Eleanor Warner[1], Ian Norton[1] and Tom B Mills[1]

[1]School of Chemical Engineering, University of Birmingham, Edgbaston Campus, Birmingham, UK B17 0JS

Correspondence to: Saumil Sudhir Vadodaria (s.vadodaria@bham.ac.uk)

ABSTRACT

Thermoreversible hydrogels are widely used in foods, drug delivery and tissue engineering. Novel shapes/textures out of them are being increasingly fabricated using Fused Deposition Modelling (FDM) type 3D printing, where gels are extruded layer-by-layer above their gelling temperature followed by cooling. It is crucial to develop a library of suitable materials and optimise printing conditions to ensure good print quality and to minimise damage to the embedded active components (cells, flavours, nutrients and drug molecules).

Several mixtures of gelatin with gellan and agar were prepared and characterised. They were formed into cylinders using FDM at four different temperatures and three different speeds. The printed specimens were tested for their mechanical properties using compression.

The fidelity of printed shapes and the inter-layer adhesion appeared to rely on the cooling required before approaching the gelling temperature and the time available for it, through printing speed. A generic printability diagram was constructed for navigating to the optimal printing conditions for a given formulation.

KEYWORDS

3D Printing, Additive Manufacturing, Hydrogels, Gelatin, Gellan, Agar

1 INTRODUCTION

The technique for creating geometrical objects through addition of layers of materials, commonly referred to as additive manufacturing (AM), has had a significant impact on many different industrial sectors including building light-weight components in the aerospace industry [1] to producing custom implants in the dental industry [2]. This research has been driven by the ability of AM to create novel shapes with complex geometries and produce little waste [3], using materials ranging from plastic, metals, ceramics, concrete and even hydrogels.

Hydrogels are represented by a wide range of water-rich materials consisting of sample-spanning rheologically significant network of macromolecules. Hydrogels with biopolymers are widely used in food and healthcare for their high water retention and textural resemblance to many foods as well as natural tissues [4–6].

Much of the recent research in 3D printing of hydrogels has been focused on food and tissue engineering. Within the food industry, fabrication of objects through the use of AM has been propelled by the ability to create foods with elaborate textures and a tailored nutritional content [7]. To date, a large amount of research has been conducted on edible materials that hold their shape after extrusion due to their yield stress, such as doughs and pastes [8,9].

Within healthcare applications in general and bioprinting in particular, the hydrogels act as a surrogate for housing biomaterials such as drug molecules, proteins, cells and growth factors [4]. The applications for such hydrogels range from as drug delivery vehicles to tissue fabrication.

An important subset of hydrogels is thermoreversible gels, i.e. the hydrogels with a critical temperature below which the material forms a gel, and are generally processible above that temperature. Under Fused Deposition Modelling (FDM), a type of AM, thermoreversible hydrogels are extruded above their gelation temperature and deposited in a layer-by-layer fashion, followed by the cooling below the gelation temperature defining the printed shape. Besides their easily tuneable gelation process, their ability to mostly achieve high shape fidelity makes them an interesting topic for investigation [10].

It is apparent that printing temperature as well as printing speed are key variables during FDM of thermoreversible gels. For example, too low of a printing temperature may cause the material to gel within the nozzle, while too high of the temperature may delay the cooling and therefore gelation. Similarly, printing speed would greatly influence the time available for cooling prior to deposition of the subsequent material layer.

Besides the obvious requirement of maintaining shape against gravity, 3D printing of thermoreversible hydrogels is subject to more conditions with regards to tissue engineering. While a very high degree of cross-linking density brings with it better shape fidelity, it often also results in a limited growth, differentiation and migration of cells [11]. The gelation process within the hydrogel must not harm the embedded cells. More crucially, FDM of cell-laden thermoreversible gels can potentially damage cells through elevated temperatures [4,10]. Also, shear flow through a nozzle during extrusion subjects the cells to shear rate and shear stress, an excess of which can rupture the membranes of some cells while altering the behaviour of the surviving cells [12]. Such phenomena may even be relevant for printing of edible thermoreversible gels, as the flavours and nutrients may undergo irreversible chemical changes at high temperature and the texture responsible for sensory perception (as dictated by gel microstructure) is influenced by the applied shear rate through printing speed.

The reality of perceived 'ideal' printing temperature and speed being determined by not only the properties of the thermoreversible hydrogel matrix but also by the limitations of active components (flavours, nutrients, cells etc.) embedded within it, makes their FDM process rather challenging. Such 'ideal' range of printing parameters is best visualised as an intersection of parameters suited to (i) the active components and (ii) the gel matrix. The parameters suited to the active components can be determined separately and are beyond the scope of the current study.

In the present investigation, the aim is to characterise several thermoreversible gel formulations for their thermal and rheological properties, and to fabricate shapes using them through the FDM process at various temperatures and printing speeds. These shapes will then be tested for their appearance as well as their mechanical properties. These results will reveal how a specific combination of material properties and printing parameters influences the printing quality. Based on these, the set of printing parameters can be identified in order to achieve a specifically desired texture and appearance of the printed object.

Gel formulations comprising gelatin, gellan and agar will be used as model materials for the study. They are all thermo-reversible polysaccharides commonly used in the food industry as well as tissue engineering. Gelatin is a product obtained via the partial hydrolysis of collagen, which is derived from animal skin and bones [13]. Gelation of gelatin solution occurs through the transition of random coils to helices as the temperature is reduced [14]. Gelatin is one of the most used hydrocolloids globally due to its properties such as its low melting temperature (which gives it a 'melt in the mouth' sensory perception), its high viscosity and high gel strength [15].

However, the low-melting temperature of gelatin significantly limits its potential for applications in which the human body temperature of 37°C degree is of relevance. Many formulations containing gelatin have melting temperature lower than 37°C, which renders them unfeasible for tissue engineering. One of the approaches to overcome this is to chemically modify and subsequently cross-link gelatin [10]. This approach may make the formulation vulnerable to the potential toxicity of the cross-linking agents. In the present study, the strategy to raise the melting temperature of gelatin relied upon its complexation with other biopolymers. This alters the nature of cross-linking from chemical to physical, and avoids the presence of synthetic cross-linking agents altogether.

Gellan gum is a linear extracellular polysaccharide which is composed of repeating tetrasaccharide units [16]. Upon the addition of gellan to gelatin, the gellan may form a coupled network with gelatin wherein the anionic domains of gellan form new heterolytic junction zones with cationic domains of gelatin molecules leading to increases in gelation temperature, gelation rate and gel strength [17,18].

Agar is extracted from certain marine algae [19] and its structure comprises of 1,3-linked, D-galactose and 1,4-linked, 3,6-anhydrogalactose [20]. Agar gives brittle gels and forms coacervates when mixed with gelatin. The mixture separates in two liquid phases, i.e. coacervate phase and supernatant phase. Although immiscible, these phases coexist in thermodynamic equilibrium [21]. In the mixture gel of gelatin and agar, the network formation of one of the components is hindered in part by the other component [22,23].

It is expected that the trends observed in the relationship between the printing parameters and printing quality of the thermoreversible gels mentioned above may hold for many other gels of the same type.

2 EXPERIMENTAL

2.1 Materials

Porcine gelatin (250 bloom), low acyl gellan gum and agar were purchased from Sigma-Aldrich (UK). The materials were used without any purification or modifications.

2.2 Sample Preparation

Seven different samples were prepared in total: 5% (w/w) gelatin with 1, 2 and 3% (w/w) gellan and 5% (w/w) gelatin with 1, 2 and 3% (w/w) agar. Also included was the 5% gelatin (w/w) sample with no other additives.

The samples of 5% gelatin and 1, 2, and 3% gellan were prepared by dispersing the required amount of gellan into the deionised water at a temperature of 85˚C on a heated bed under agitation using a magnetic stirrer bar for 30 minutes. Subsequently, the gelatin was added to the solution at a temperature of 60˚C, and left to hydrate for 30 minutes.

The formulations with agar were prepared in a similar way. However, the water was initially heated to 90˚C before dispersing the agar under agitation. The 5% gelatin only sample was prepared by adding gelatin to water at 60°C.

Henceforth, the 5% gelatin sample will be referred to as G5. The samples containing 5% gelatin and 1, 2 and 3% of gellan will be named as G5G1, G5G2 and G5G3 respectively. Similarly, the samples with 5% gelatin and 1, 2 and 3% of agar will be termed as G5A1, G5A2 and G5A3 respectively.

2.3 Determination of material properties

2.3.1 Calorimetry

In order to detect the thermal transitions of the formulations, approximately 0.7 g of each sample was loaded into a stainless-steel cell. The reference cell was filled with the same amount of deionised water. The samples were loaded into Seteram μDSC 3 evo (Seteram, France) at a temperature of around 25˚C. The temperature was

then set to 0˚C and was held there for about 60 minutes. The samples were then tested using the following profile: initially a heating ramp was applied at a scanning rate of 1.2˚C/min, up to a temperature of 55˚C for the samples with gellan, and 95˚C for the samples with agar. The samples were then immediately cooled at the same rate back to 0˚C. The samples were then held there for a further 60 minutes. The gelling and melting temperatures were determined as the onset of the peaks.

2.3.2 Rheometry

The rheological measurements were undertaken on a Kinexus pro rheometer (Malvern, UK), using a serrated parallel plate with 60 mm diameter and 1 mm measurement gap. This geometry was employed in order to avoid slippage of the samples. A small amount of silicon oil was spread around the rim of the geometry, in order to minimise the evaporation of the samples. All of the samples were loaded at 60˚C. Once the testing temperature was reached, the samples were then allowed to rest for 5 minutes in order to allow them to equilibrate.

Oscillatory amplitude (strain) sweep tests were performed for all samples at 1Hz of constant frequency. 1% strain was found to be within the respective linear viscoelastic regions of all samples where phase angle δ was found to be constant. This value was used when undertaking all further rheological experiments in this study.

G' (storage modulus) and G'' (loss modulus) were measured as a function of temperature at a constant frequency of 1 Hz and the oscillatory strain of 1%. From an initial temperature of 60˚C, the samples were cooled at a rate of 1˚C/min to a final temperature of 20˚C. Throughout the experiment, the evolution of the magnitudes of G' and G'' were recorded.

Small-amplitude (1% strain) oscillatory frequency sweeps were also performed for all samples. The frequency was varied from 0.1 – 100 Hz at 20°C and the magnitudes of G' and G" were recorded.

2.4 Fused Deposition Modelling

The 3D printer employing a FDM technique used within this study was created by modifying a commercially available Hictop Prusa i3 plastic printer with a custom-built syringe pump, which has been documented in detail by [24].

To summarise, cylindrical shapes of 22 mm diameter and 40 mm height were printed, with each individual layer 0.3 mm thick. The needle with 0.6 mm of internal diameter was used to extrude the material. Temperature control and insulation system were in place in order to ensure the right temperature both within the syringe barrel and the nozzle. The cylinders were printed at 45, 50, 55 and 60°C temperatures and at 10, 25 and 50 mm/s printing speeds. These printing speeds correspond to the volumetric flow rates of approximately 9.39×10^{-9}, 2.26×10^{-8} and 3.66×10^{-8} m^3/s respectively.

For comparison, 'control' samples with identical dimensions were prepared by casting the molten samples in a 3D printed mould at respective temperatures and were allowed to cool for an hour prior to characterisation.

2.5 Textural analysis

A texture analyser, TA.XT Plus (Stable Micro Systems Ltd., UK) was used in order to characterise the mechanical properties of the cylindrical specimens using a compression test. Cast and printed samples of the formulations were tested for comparison purposes. The printed specimens created at each of the different printing temperatures and speeds were also left for an hour before testing. The one hour waiting period was conducted in order to allow the formulations time to gel together, in accordance with [17] who investigated the gelation of gelatin and polysaccharide samples and determined that the extent of gelation began to plateau after approximately 1 hour.

A 40 mm diameter cylindrical aluminium probe was employed, and the majority of the experiments were undertaken using a 5-kg load cell to measure the force. Due to the high strength of the gellan-containing cast samples, a 30-kg load cell was used. The compression rate was maintained at 2 mm/s and the measurements were undertaken to a strain compression of 50%, using a trigger force equivalent of 10 g under gravity.

Before the experiments, a thin layer of silicone oil was applied to the plates in order to reduce the friction during compression. The data presented is a mean of at least 5 replicates with ± one standard deviation.

3 RESULTS AND DISCUSSION

3.1 Thermal Properties

The first heating and cooling cycles for the gellan-containing samples can be seen in Figures 1 (A) and (B) respectively. For the heating curves of the formulations with the addition of gellan, there appears to be only one endothermic peak. This is due to the endotherms for helix-coil transition of both the gelatin and gellan overlapping. Compared to the endothermic peak for just the gelatin alone, the gellan containing formulations display a larger shoulder on the right of the peak indicating the transition of the gellan similar to those found by [25].

In Figure 1 (B), two distinct exothermic peaks can be seen for each of the formulations with the addition of gellan on their respective cooling curves. The broad peak, spanning 10-20˚C can be attributed to the gelation of the gelatin. The secondary peak occurring at a temperature around 37˚C can be attributed to the helix-coil transition of the gellan molecules, which is also in accordance with the observations by [25].

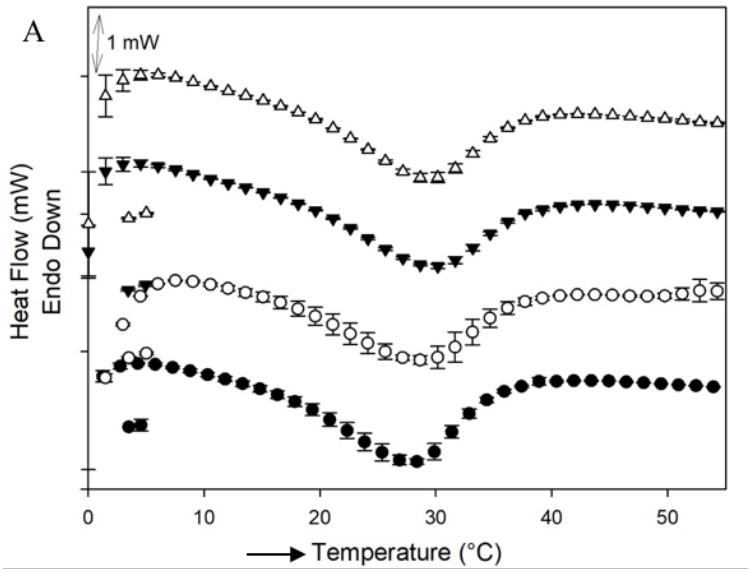

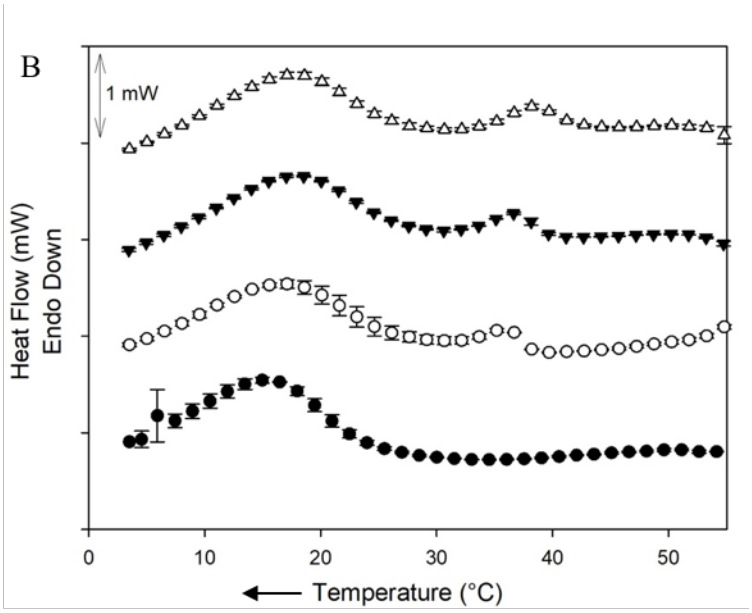

Figure 1. µDSC heating (A) and cooling (B) profiles for G5 (●), G5G1 (○), G5G2 (▼) and G5G3 (△). (n=3, error bars represent one standard deviation).

The second and third heating and cooling cycles of the gellan-containing samples were extremely similar to the curves shown, indicting there were no irreversible changes upon cooling and heating.

The first heating and cooling cycles for agar-containing samples can be seen in Figures 2 (A) and (B) respectively. Two endothermic and two exothermic peaks are apparent for all of the agar-containing formulations. The broader peaks for both the endotherm and exotherm can be attributed to the gelation of gelatin within the formulation, similar to the results reported in the earlier literature [26].

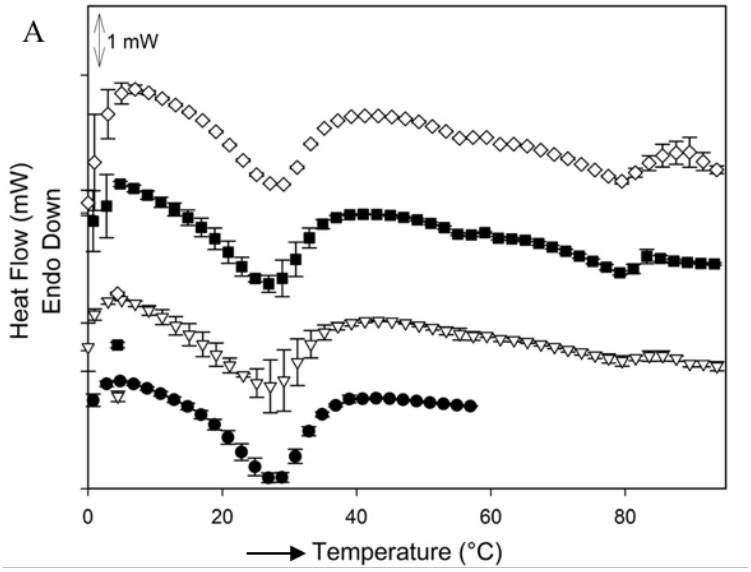

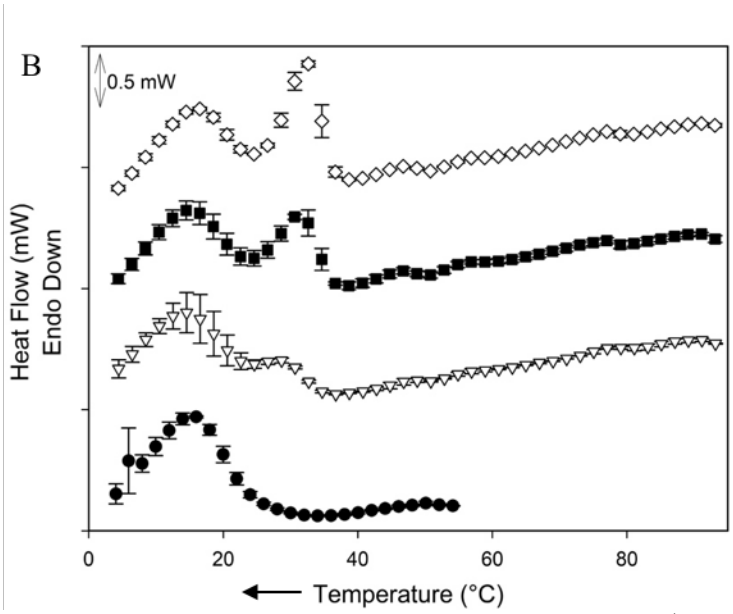

Figure 2. µDSC heating (A) and cooling (B) profiles for G5 (●), G5A1 (▽), G5A2 (■) and G5A3 (◇). (n=3, error bars represent one standard deviation).

The second peaks (at approximately 80˚C on the endotherm and 40˚C on the exotherm), can be attributed to the melting and setting of the agar respectively via the helix-coil transitions which are similar to results found by [27]. The sharp peak of gelation for the agar manifests the cooperative conformational transition as compared to the ongoing structure development of the gelatin network, which is the broader peak [28].

A significant temperature hysteresis of agar is seen with melting occurring around 80˚C, while gelation occurs closer to around 40˚C. These are similar to the typical melting and gelling temperature of agar [29]. As expected, the size of the peak attributed to the agar for both heating and cooling increased with the concentration of agar. Also, a slight increase was observed in the observed gelation temperature with agar concentration, in agreement with [30].

The second and third heating cycles for all agar-containing formulations were extremely similar to the curves shown, indicating that there were no irreversible changes upon heating and cooling.

The thermal properties of these materials were further explored by performing temperature sweeps using a rotational rheometer in accordance with [31].

G’ and G’’ were measured at constant oscillatory strain and frequency, at varying temperature. The measurement data for the formulations with gelatin and gellan as well as with gelatin and agar are shown in Figures 3 and 4 respectively.

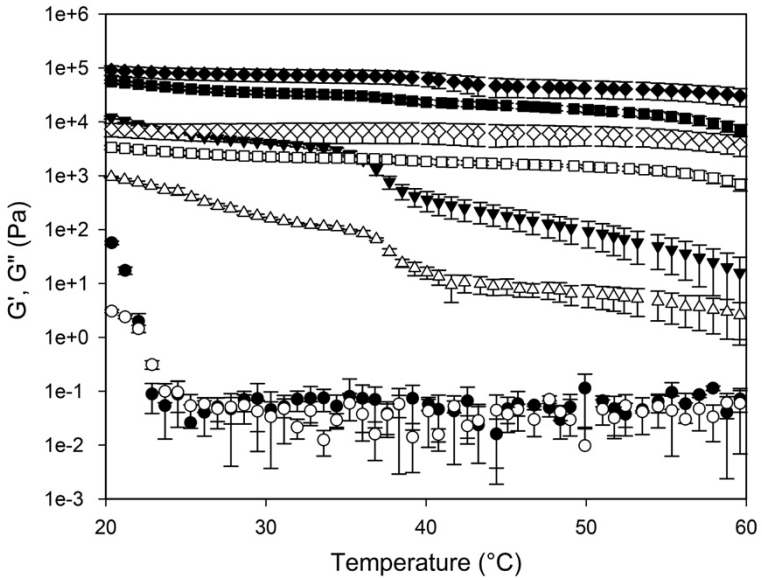

Figure 3. Temperature sweep data for G5 (○), G5G1 (▽), G5G2 (□) and G5G3 (◇). Open symbols are the G", while closed symbols are the G'. (n=3, error bars represent one standard deviation).

From Figure 3, it can be seen that throughout the range of temperatures tested for all of the gellan-containing formulations, G' is always greater than G". This suggests the inter-polyelectrolyte complex formation between gelatin and gellan leads to a physical cross-linked network which is distinct from the network of gelatin alone (Zheng et al., 2018). There is a clear G' inflection point for G5G1 at a temperature of approximately 38˚C. G' for G5G2 and G5G3 have slightly less pronounced inflections at temperatures of approximately 41 and 42˚C respectively.

In the absence of cross-over point of the moduli, [32] used the inflection point of the G' as the gelling temperature while investigating the effect of the concentration of gellan on its viscoelastic properties.

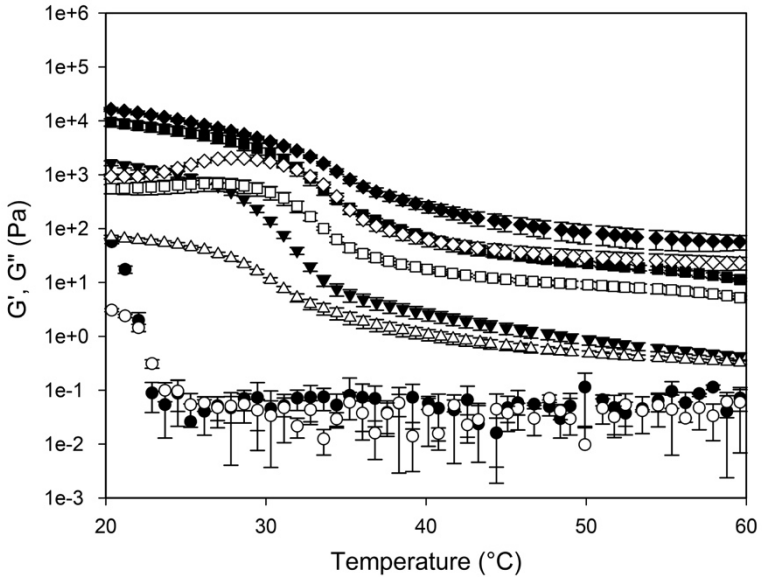

Figure 4. Temperature sweep data for G5 (○), G5A1 (▽), G5A2 (□) and G5A3 (◇). Open symbols represent G", while closed symbols represent G'. (n=3, error bars represent one standard deviation).

A similar phenomenon was seen with the agar-containing formulations. G' was greater than G" at all of the temperatures tested as shown in Figure 4, thus indicating that the material was predominantly elastic over the whole range of temperature tested. As the temperature was reduced, the magnitude of G' gradually increased until the respective inflection points where G' increased relatively quicker. These inflection points were close to

the gelation temperature determined from the µDSC. Such G' inflection was also observed by [30] who investigated the sol-gel transition of fish gelatin and agar.

In both gellan- and agar-containing mixtures, the dependence of G' on temperature decreases with increasing concentration. Also, such dependence is greater for agar-containing formulations compared to gellan-containing formulations.

As there were no cross-over temperatures from the temperature sweeps and the inflection points were not always sharp, the gelling temperatures were determined as the onset of the curve from the µDSC and have been summarised in Table 1. It is noteworthy that all gellan-containing formulations have their gelling temperature above 37°C, this is true for only one of the agar-containing formulations.

Sample	Gelling Temperature from Onset of Exotherm / °C
G5G1	39 ± 0.005
G5G2	40 ± 0.01
G5G3	42 ± 0.01
G5A1	36 ± 0.005
G5A2	37 ± 0.02
G5A3	38 ± 0.01

Table 1. Gelling temperatures from the onset of exotherm for gellan and agar-containing samples.

3.2 Rheological Properties

G' and G'' are relevant linear viscoelastic parameters in order to characterise the ability of materials to retain their printed shape under gravity while cooling down to the ambient temperature following extrusion. For this purpose, oscillatory frequency sweeps were conducted on all of the formulations at 20˚C (data shown in supporting information). For all mixed samples, the values of G' were higher than G'' by more than one order of magnitude. Also, both moduli for all of the formulations were nearly frequency independent, indicating that the materials were in a visco-elastic solid-like state [33]. Moreover, with the concentration of either of the secondary biopolymer, the magnitude of G' and G'' increased due to the formation of an increasingly stronger and rheologically significant network of inter-polyelectrolyte complex. This is in agreement with reported literature for mixtures of gelatin with gellan [17] and with agar [34] as the secondary biopolymers.

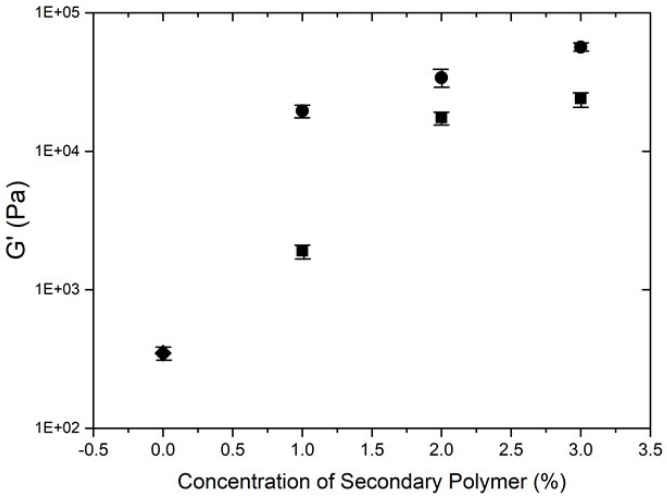

Figure 5. G' at 1Hz and 20˚C of 5% gelatin only (◆), as well as 5% gelatin and various amounts of gellan (●) and agar (■) (n=3, error bars represent one standard deviation).

In order to compare all the formulations, representative values of G' were taken at 1Hz oscillation frequency for each of the formulations and were plotted as a function of the secondary biopolymer concentration as shown

in Figure 5. At each concentration of the secondary biopolymers, the magnitude of G' was larger for the formulations with gellan then agar.

It is important for the materials to possess a sufficiently high G' in order to maintain fidelity in the printed shape [35]. G' also partly governs how fast the material will spread after being extruded onto the print bed.

3.3 Printability – Visual Appearance

In order to determine the printability of gellan and agar-containing formulations, cylinders were printed at different temperatures (45, 50, 55 and 60˚C) and speeds (10, 25 and 50 mm/s). The formulations with agar printed at a temperature of 55˚C displayed a large amount of material spreading. It was thus deemed unlikely they would be printable at higher temperatures and were not printed at 60°C.

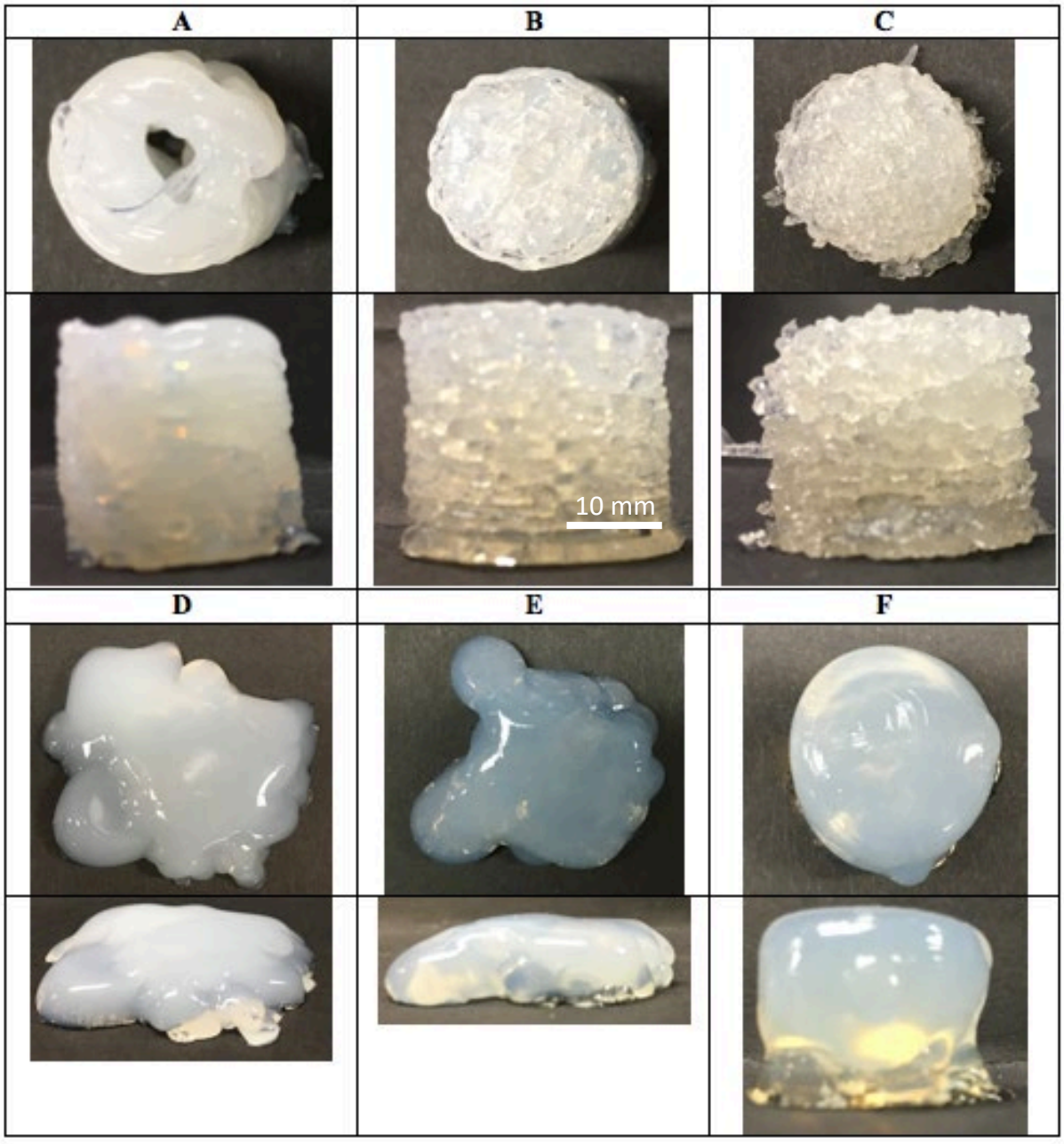

Figure 6. Printed cylinders of G5G1 (A, D), G5G2 (B, E) and G5G3 (C, F) at 45˚C and 10 mm/s (top row) and at 60˚C and 50 mm/s (bottom row).

Figure 6 displays the representative cylinders printed using gellan-containing mixtures at the two extreme printing parameters: 45˚C and 10 mm/s (top row) as well as 55˚C and 50 mm/s (bottom row). They are the two

extremes in the sense that the first set of conditions provides the longest time for cooling from a lower temperature while the second set offers the shortest time for cooling from a higher temperature.

It can be seen that partial delamination of all gellan formulations occurred with the cylinders printed at the lowest printing temperature and speed. This indicates that the formulations were gelling within the nozzle and were extruded semi-solid. This gave rise to delaminated layers as the layers gelled prior to having a sufficient adhesion to the neighbouring layers. The delaminated layers are increasingly visible with increasing concentration.

[36] also noted such partial delamination, and determined that pre-mature gelation during extrusion prior to contact with the subsequent layer must be prevented in order to produce a well-defined shape. This phenomenon of delamination also occurs when printing in plastic [37]. Hence, this set of temperature and speed is unsuitable for printing cohesive shapes with these formulations despite the desired cylindrical shape was achieved for all gellan-containing formulations.

At the highest printing temperature and speed, it can be seen that cylinders printed using G5G1 and G5G2 resulted in complete collapse, due to their low magnitude G'. Similar observation was reported by [38] where a hydrocolloid mixture of κ-carrageenan, xanthan gum and starch was printed at a temperature significantly above its gelling temperature. This hydrocolloid mixture was unable to support its post-printed shape against gravity as a result of failure to recover its mechanical strength in a short period of time.

On the other hand, the cylinder printed with G5G3 was observed to maintain a cylindrical shape owing to its higher G'. As shown in Figure 3, the formulations have significantly lower G' at 60°C temperature, often by more than an order of magnitude compared to the G' at 20°C. A longer time is required for a given formulation to cool down to near 20°C temperature from 60°C (thereby recovering its G' sufficiently to maintain its post-extrusion shape), and that time may not be available at the highest of printing speed.

The cylinders printed with gellan-based formulations displayed relatively well-defined shapes at many of the intermediate printing temperatures and speeds (pictures not shown).

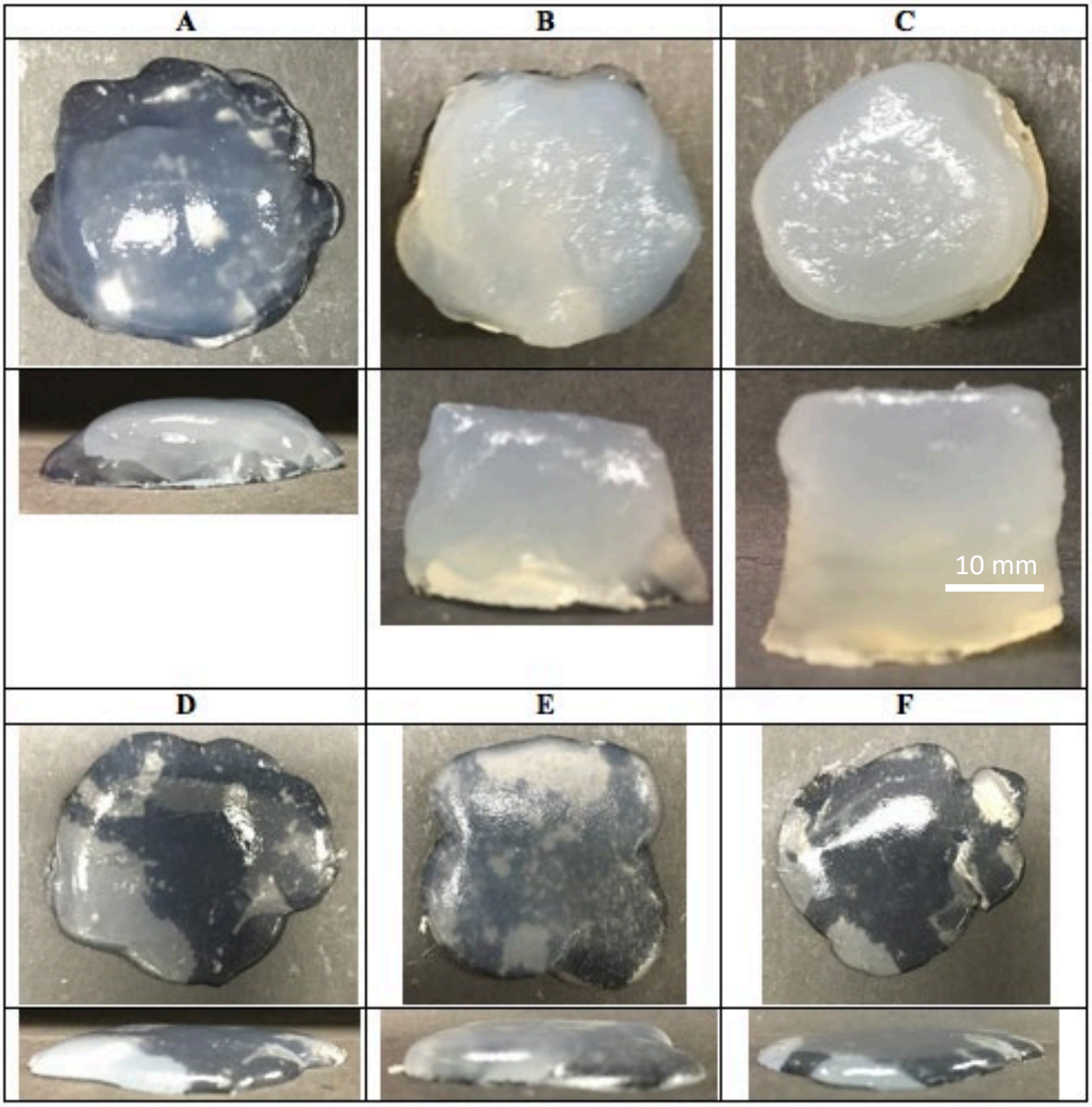

Figure 7. Printed cylinders of G5A1 (A, D), G5A2 (B, E) and G5A3 (C, F) at 45˚C and 10 mm/s (top row) and at 55˚C and 50 mm/s (bottom row).

Figure 7 displays the representative cylinders printed with agar-containing samples at the two extreme printing parameters: 45˚C and 10 mm/s (top row) as well as 55˚C and 50 mm/s (bottom row).

At the lowest printing temperature and speed, sample G5A1 displayed large amounts of pooled material as opposed to a cylinder. On the other hand, G5A2 and G5A3 displayed relatively more cylinder-like printed shapes. As the printing speed and temperature were increased, the material spread significantly and the heights of the cylinders did not reach the minimum threshold in order to be classed as printable.

None of the agar-containing mixtures at the higher printing temperature and speed displayed signs of being able to retain the printed shape. Once the material was extruded from the nozzle, it created pools instead of a cohesive shape. This lack of ability to retain their shape is likely due to relatively low G' of agar-containing formulations, particularly at higher temperatures.

The aesthetic appearance of printed specimen deteriorated further as the printing temperature and speed increased. Lower magnitude of G' for agar containing formulations led to the cylinders not achieving the desired height as the extrudate spread to a larger diameter than intended.

Since the pictures of printed specimen are numerous and the printing quality is subjective, it is necessary to adopt an indexing approach by ascribing them with colour codes analogous to traffic-light. The traffic-light chart of printability for all of the cylinders printed at each of the different printing temperatures and speeds, using all of the different formulations can be seen in Figures 8 and 9. Printed cylinders with a height over 98% of the intended height were defined as well printed (highlighted in green). The cylinders printed with a height between 98 – 95% of the intended height were classified as almost printed (highlighted in orange) and with printed cylinders whose heights were below 95% of the intended, the cylinders were considered as not printed well (highlighted in red). Furthermore, Roman numerals I, II and III were used to elaborate the morphology, i.e. complete collapse, partial collapse and partial delamination respectively.

A

Speed (mm/s)	Temperature (°C) 45	50	55	60
10	III			II
25	II	II	I	I
50	I	I	I	I

B

Speed (mm/s)	Temperature (°C) 45	50	55	60
10	III			II
25	III		II	II
50	III	II	II	I

C

Speed (mm/s)	Temperature (°C) 45	50	55	60
10	III	III		
25	III			II
50	III	II	II	II

Figure 8. Traffic-light chart of printability at different temperatures and speeds of G5G1(A), G5G2 (B) and G5G3 (C). Green indicating that it had printed well, orange indicating that it had printed satisfactorily and red indicating that it had not printed well. The roman numerals describe: complete collapse (I), partial collapse (II) and partial delamination (III).

The cylinders printed at the highest temperatures and speeds with the formulations of gelatin and gellan did not meet the required minimum height. This was due to the materials dripping spontaneously out of the nozzle. When the printing temperature and speed were reduced, the printed cylinders achieved better height and were considered printable. This was possibly due to the lower speeds and lower temperatures allowing the temperature to easily approach ambient during cooling, maximising the recovery of G'.

It is noteworthy that at the lowest printing speed of 10 mm/s, the minimum printing temperature to ensure a well-printable cylinder has to be at least 6°C above the respective gelling temperature of the formulation. This is due to premature cooling/gelling of the extrudate hindering a good adhesion with the subsequently printed layer in case of a small difference of temperature. However, a lower temperature difference can still be imposed to print a good quality cylinder as long as the printing speed is also higher, reducing the time available for premature cooling. On the other hand, low temperature and even higher speeds often caused surface irregularities on the extruding filament, presumably owing to high flow rate being experienced in the nozzle by a cooler and hence relatively stiffer material, giving rise to rheological instabilities such as shear fracture.

As previously mentioned, it can be seen that none of the formulations of gelatin and agar could be considered well-printed or almost printed. However, the associated morphological descriptors still indicate that at least shorter cylindrical shapes were formed at the lowest temperature as well as low and intermediate speeds using the samples G5A2 and G5A3. This is likely due to the lowest temperature and lower speeds providing ample opportunity for the recovery of G'.

A

Speed (mm/s)	Temperature (˚C) 45	50	55	60
10	I	I	I	
25	I	I	I	
50	I	I	I	

B

Speed (mm/s)	Temperature (˚C) 45	50	55	60
10	II	I	I	
25	II	I	I	
50	I	I	I	

C

Speed (mm/s)	Temperature (˚C) 45	50	55	60
10	II	I	I	
25	II	I	I	
50	I	I	I	

Figure 9. Traffic-light chart of printability at different temperatures and speeds of G5A1(A), G5A2 (B) and G5A3 (C). Green indicating that it had printed well, orange indicating that it had printed satisfactorily and red indicating that it had not printed well. The roman numerals describe: complete collapse (I), partial collapse (II) and partial delamination (III).

3.4 Printability – Mechanical Properties

In order to determine how well the layers within printed cylinders gelled together, their mechanical properties were tested using a compression test via a texture analyser. Initially, such tests on cast cylindrical samples of all of the formulations were performed in order to estimate how strong the formulations were when formed through pouring into a mould, resulting in no defined layers (i.e. 'control' samples). While one of the drawbacks of mechanical testing is a relatively high uncertainty compared to many other quantitative techniques, it is still useful for gaining relevant information about the microstructure of hydrogels.

Figure 10 shows the peak force values of the cast cylinders of gelatin with various concentrations of secondary biopolymers gellan and agar. As the concentration of the secondary biopolymer increased for all of the formulations, the peak force increased (except for a small decrease between the formulations with G5A1 and G5A2). This phenomena was also observed by [39] who investigated mixtures of gelatin and gellan and [40] who investigated blends of gelatin and agar. The peak force values of agar-containing samples were considerably lower than those with gellan, reflecting the trends from rheological measurements.

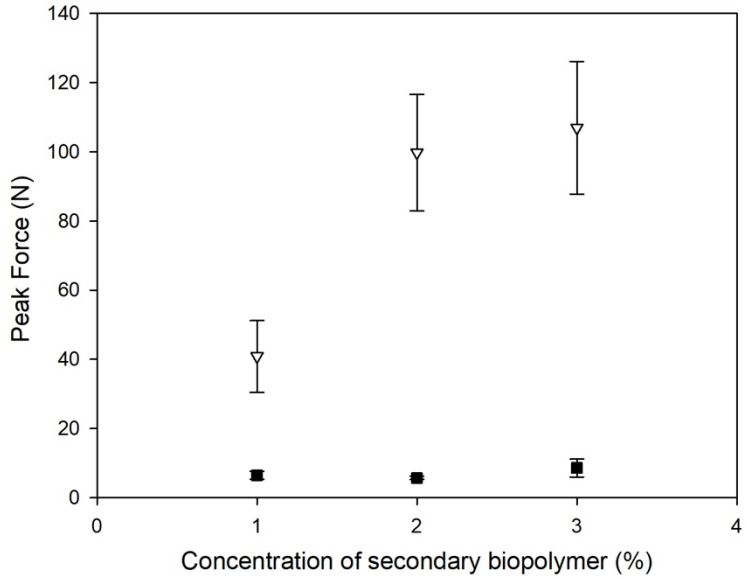

Figure 10. Peak force values of cast cylinders of 5% gelatin with gellan (▽) and agar (■) at various concentrations of the latter two (n≥5, error bars represent one standard deviation).

The results of the peak force tests at different printing speeds and temperatures for the formulations of gellan-containing samples are shown in Figure 11 (A), (B) and (C) respectively. As none of the formulations with agar were regarded as printable, they could not be tested for their peak force.

For G5G1, the peak force increased with the printing temperature. Higher melt temperature leads to better adhesion between the successive layers, resulting in stronger parts [41] unless the temperature is too high for the G' of the specimen to sufficiently recover and to hold its shape.

When printing at the lowest temperature (45˚C), G5G2 and G5G3 successfully printed at all three printing speeds tested, with the strongest cylinder printed at the fastest speed (50 mm/s) and weakest cylinder printed as the slowest speed (10 mm/s). This echoed the findings from their visual appearance that the faster printing speed led the layers to have less time for premature gelling while subsequent layers were being deposited. This enabled each layer to be fused efficiently with the neighbouring layers, making the printed shape stronger [42].

Unsurprisingly for both formulations, an increase in the printing temperature also resulted in higher peak force measurements at constant printing speed (where the cylinder could still be printed) due to an increase in the interlayer adhesion between the layers, for reasons similar to the abovementioned. Such trends were also observed by [43] for thermoplastics.

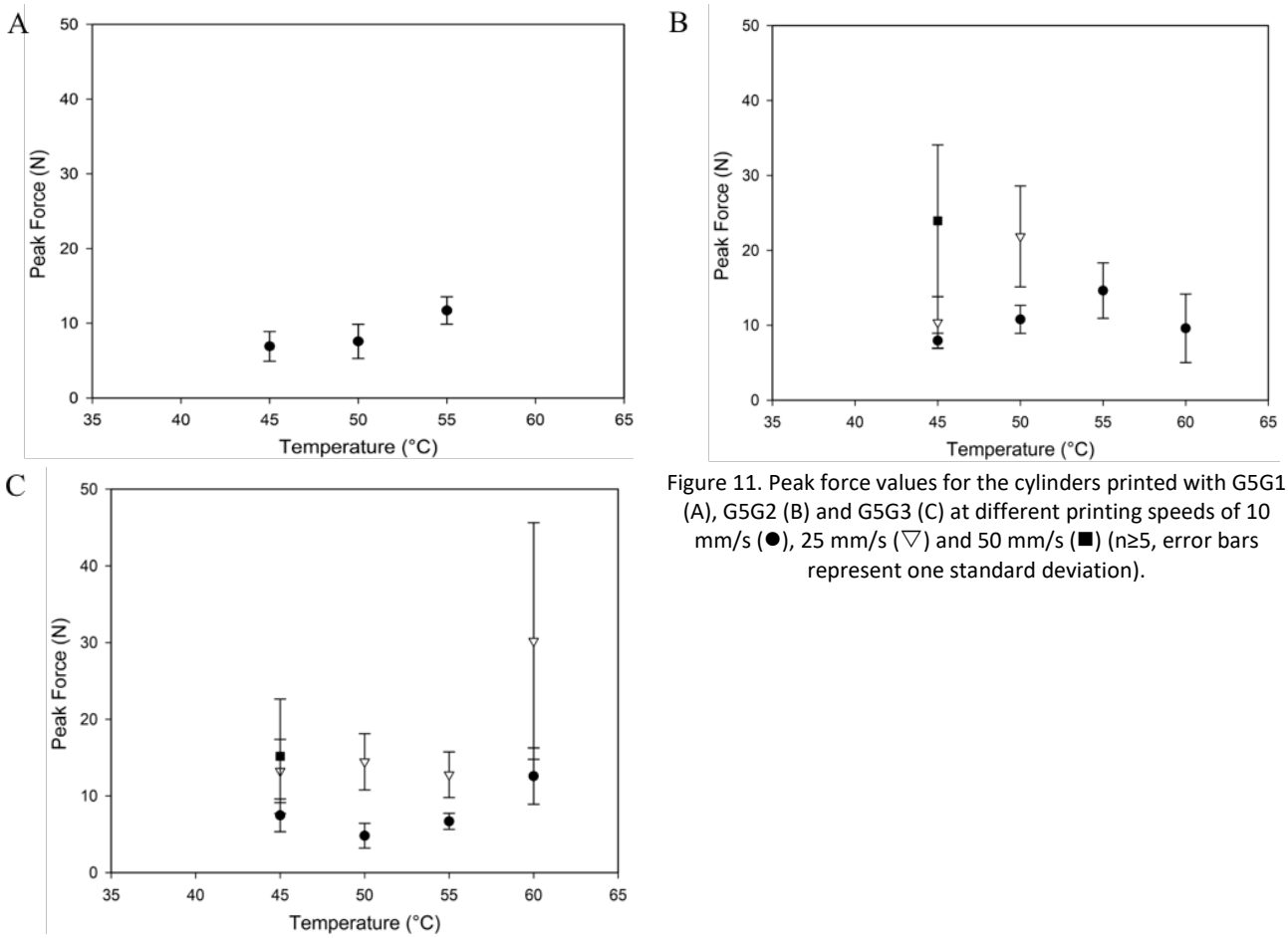

Figure 11. Peak force values for the cylinders printed with G5G1 (A), G5G2 (B) and G5G3 (C) at different printing speeds of 10 mm/s (●), 25 mm/s (▽) and 50 mm/s (■) (n≥5, error bars represent one standard deviation).

However, when both temperature and speed are high beyond a certain limit, the printability is compromised due to either (a) the printed layers spreading away prior to deposition of the subsequent layers or (b) the printed layers being unable to bear the weight of the layers above them and crumbling. Both these reasons are symptoms of poor G' recovery during post-extrusion cooling.

The peak force values for all the printed cylinders were considerably lower than those of the cast cylinders (i.e. 'control' samples) of the same formulation. Due to the nature of layer by layer manufacturing, the printed shape is expected to have weaker points at each of the layer interfaces, unlike the samples prepared by casting. Even a single inter-layer joint is sufficient to reduce the peak force. With many layers a 3D printed object normally contains, the reduction in peak force is more profound. Inferior mechanical properties of 3D printed milk protein formulations compared to their non-printed equivalents (as measured by compression test) have been reported earlier [9]. The peak force values for the gellan-containing printed cylinders are between 13 - 23% of those of their respective cast samples. Higher values of peak force for printed samples were believed to correlated with stronger inter-layer adhesion.

3.5 Generic Printability Diagram

The printability trends observed in Figures 8 and 9 with respect to temperature and printing speed as well as their correlation with the peak force measurement data can be distilled into a generic printability diagram proposed in Figure 12. This helps visualise how the optimal printing conditions for any formulation are within a certain printing temperature and speed range. This diagram can be used as a navigating tool for optimal printing conditions for any new formulation to be printed using FDM. This is achievable by mapping the print quality at a given set of printing conditions and assign the diagram the values of temperature and speed.

However, it must be noted that the boundaries between different areas in the diagram are merely for illustrative purposes. These boundaries should be interpreted with the realisation that in practice, the printing quality as a function of the two parameters in question mostly changes continuously as opposed to abruptly.

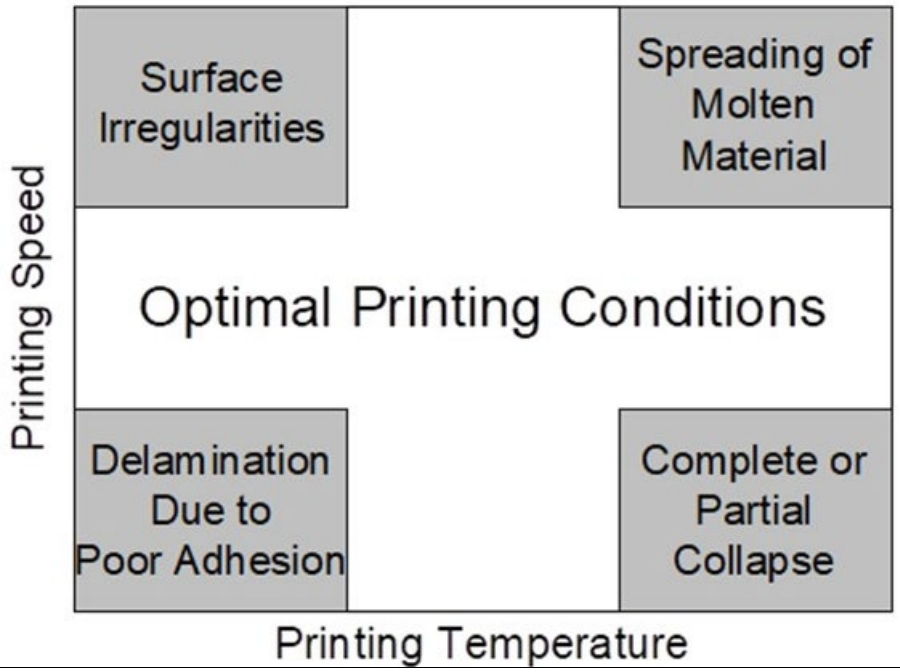

Figure 12. Generic printability diagram. Grey regions indicate extreme printing parameters leading to inadequate printing quality.

4 CONCLUSIONS

Several mixtures of gelatin and gellan as well as gelatin and agar were formulated as 'inks' for FDM. They were characterised for their thermal and rheological properties. The mixtures containing gellan were found to have higher gelling points as well as higher G' and G'' compared to the agar containing mixtures at equivalent concentrations.

G' and G'' of all the formulations were found to be temperature dependent, i.e. they increased with decreasing temperature. This temperature dependence was more profound at low concentrations of secondary biopolymers gellan and agar compared to that at higher concentrations.

The mixtures were printed into cylindrical shapes at several temperatures, all above their gelling points as well as various speeds. For gellan-containing mixtures, the printability was seen to rely on how much cooling was required (i.e. the gap between printing and gelling temperatures) and how much time was available for it (i.e. printing speed) prior to the deposition of subsequent layers. At low printing temperatures and speeds, the extrudate gelled on its own too much for it to be able to co-gel with the neighbouring layers. This led to printing of the desired shape but poorly adhered and distinctly visible layers. At higher speeds and/or temperatures, the premature gelling was minimised and partial diffusion of neighbouring layers into one another was achieved, leading to better cohesion and surface appearance. At even higher temperatures and speeds, sufficient cooling (and therefore sufficient G') could not be achieved. This led to either (i) spreading of the extrudate prior to the deposition of subsequent layer or (ii) insufficiently gelled layer(s) collapsing following the deposition of subsequent layer. No agar-containing formulations were deemed as printable.

Printed cylinders, along with the cylinders made by casting into a mould were tested for their mechanical properties. The cylinders with distinctly visible layers had lower peak force values for compression, as opposed to the cylinders with well-fused layers with relatively higher values. All printed cylinders had lower peak force values compared to their cast (i.e. 'control') counterparts. Based on the visual appearances of printed cylinders and their mechanical behaviour, a generic printability diagram was constructed.

Overall, this data can be used to 'fast-track' the use of these materials to a specific application (such as in a food product, tissue engineering or drug delivery system). Increased shape quality can be gained by further fine tuning the printer parameters but this is best done with a specific application/geometry in mind. The developed diagram could be used for mapping printing quality as a function of FDM printing parameters such as temperature and speed for any given future formulation.

5 Funding Source

This research was funded by the Engineering and Physical Sciences Research Council (EP/N024818/1).

6 REFERENCES

[1] I.J. Petrick, T.W. Simpson, 3D printing disrupts manufacturing, Res. Technol. Manag. 56 (2013) 12–16. doi:10.5437/08956308X5606193.

[2] A. Dawood, B.M. Marti, V. Sauret-Jackson, A. Darwood, 3D printing in dentistry, Br. Dent. J. 219 (2015) 521–529. doi:10.1038/sj.bdj.2015.914.

[3] D. Bak, Rapid prototyping or rapid production? 3D printing processes move industry towards the latter, Assem. Autom. 23 (2003) 340–345. doi:10.1108/01445150310501190.

[4] D.M. Kirchmajer, R. Gorkin, M. In Het Panhuis, An overview of the suitability of hydrogel-forming polymers for extrusion-based 3D-printing, J. Mater. Chem. B. 3 (2015) 4105–4117. doi:10.1039/c5tb00393h.

[5] Z. Zhang, R. Zhang, Q. Tong, E.A. Decker, D.J. McClements, Food-grade filled hydrogels for oral delivery of lipophilic active ingredients: Temperature-triggered release microgels, Food Res. Int. 69 (2015) 274–280. doi:10.1016/j.foodres.2015.01.004.

[6] H. Khalesi, W. Lu, K. Nishinari, Y. Fang, New insights into food hydrogels with reinforced mechanical properties: A review on innovative strategies, Adv. Colloid Interface Sci. 285 (2020) 102278. doi:10.1016/j.cis.2020.102278.

[7] F.C. Godoi, S. Prakash, B.R. Bhandari, 3d printing technologies applied for food design: Status and prospects, J. Food Eng. 179 (2016) 44–54. doi:10.1016/j.jfoodeng.2016.01.025.

[8] J. Lipton, D. Arnold, F. Nigl, N. Lopez, D. Cohen, N. Norén, H. Lipson, Mutli-material food printing with complex internal structure suitable for conventional post-processing, 21st Annu. Int. Solid Free. Fabr. Symp. - An Addit. Manuf. Conf. SFF 2010. (2010) 809–815.

[9] Z. Liu, M. Zhang, B. Bhandari, C. Yang, Impact of rheological properties of mashed potatoes on 3D printing, J. Food Eng. 220 (2018) 76–82. doi:10.1016/j.jfoodeng.2017.04.017.

[10] R. Suntornnond, J. An, C.K. Chua, Bioprinting of Thermoresponsive Hydrogels for Next Generation Tissue Engineering: A Review, Macromol. Mater. Eng. 302 (2017) 1–15. doi:10.1002/mame.201600266.

[11] J. Malda, J. Visser, F.P. Melchels, T. Jüngst, W.E. Hennink, W.J.A. Dhert, J. Groll, D.W. Hutmacher, 25th anniversary article: Engineering hydrogels for biofabrication, Adv. Mater. 25 (2013) 5011–5028. doi:10.1002/adma.201302042.

[12] A. Blaeser, D.F. Duarte Campos, U. Puster, W. Richtering, M.M. Stevens, H. Fischer, Controlling Shear Stress in 3D Bioprinting is a Key Factor to Balance Printing Resolution and Stem Cell Integrity, Adv. Healthc. Mater. 5 (2016) 326–333. doi:10.1002/adhm.201500677.

[13] N.A. Morrison, R.C. Clark, Y.L. Chen, T. Talashek, G. Sworn, Gelatin alternatives for the food industry, in: Phys. Chem. Ind. Appl. Gellan Gum, Springer Berlin Heidelberg, Berlin, Heidelberg, 1999: pp. 127–131. doi:10.1007/3-540-48349-7_19.

[14] C. Joly-Duhamel, D. Hellio, A. Ajdari, M. Djabourov, All gelatin networks: 2. The master curve for elasticity, Langmuir. 18 (2002) 7158–7166. doi:10.1021/la020190m.

[15] D.M. Considine, G.D. Considine, eds., Foods and Food Production Encyclopedia, 1st ed., Van Nostrand Reinhold Company, 1982.

[16] L.H. Fasolin, C.S.F. Picone, R.C. Santana, R.L. Cunha, Production of hybrid gels from polysorbate and gellan gum, Food Res. Int. 54 (2013) 501–507. doi:10.1016/j.foodres.2013.07.026.

[17] L.G. Fonkwe, G. Narsimhan, A.S. Cha, Characterization of gelation time and texture of gelatin and gelatin-polysaccharide mixed gels, Food Hydrocoll. 17 (2003) 871–883. doi:10.1016/S0268-005X(03)00108-5.

[18] Y. Zheng, Y. Liang, D. Zhang, X. Sun, L. Liang, J. Li, Y.N. Liu, Gelatin-Based Hydrogels Blended with Gellan as an Injectable Wound Dressing, ACS Omega. 3 (2018) 4766–4775. doi:10.1021/acsomega.8b00308.

[19] E.W. Flick, Emulsifying Agents - An Industrial Guide, Noyes Publications, Park Ridge, New Jersey, USA, 1990.

[20] G. Feiner, Meat Products Handbook: Practical Science and Technology, Woodhead Publishing Limited, 2006.

[21] S.S. Singh, H.B. Bohidar, S. Bandyopadhyay, Study of gelatin-agar intermolecular aggregates in the supernatant of its coacervate, Colloids Surfaces B Biointerfaces. 57 (2007) 29–36. doi:10.1016/j.colsurfb.2006.12.017.

[22] Y. Shiinoki, T. Yano, Viscoelastic behavior of an agar—gelatin mixture gel as a function of its composition, Top. Catal. 1 (1986) 153–161. doi:10.1016/S0268-005X(86)80017-0.

[23] H. Moritaka, K. Nishinari, H. Horiuchi, M. Watase, Rheological Properties of Aqueous Agarose-Gelatin Gels, J. Texture Stud. 11 (1980) 257–270. doi:10.1111/j.1745-4603.1980.tb00325.x.

[24] E.L. Warner, I.T. Norton, T.B. Mills, Comparing the viscoelastic properties of gelatin and different concentrations of kappa-carrageenan mixtures for additive manufacturing applications, J. Food Eng. 246 (2019) 58–66. doi:10.1016/j.jfoodeng.2018.10.033.

[25] E. Miyoshi, T. Takaya, K. Nishinari, Effects of salts on the gel-sol transition of gellan gum by differential scanning calorimetry and thermal scanning rheology, Thermochim. Acta. 267 (1995) 269–287. doi:10.1016/0040-6031(95)02485-9.

[26] S.S. Singh, V.K. Aswal, H.B. Bohidar, Structural studies of agar-gelatin complex coacervates by small angle neutron scattering, rheology and differential scanning calorimetry, Int. J. Biol. Macromol. 41 (2007) 301–307. doi:10.1016/j.ijbiomac.2007.03.009.

[27] M. Watase, K. Nishinari, Thermal and rheological properties of agarose-dimethyl sulfoxide-water gels, Polym. J. 20 (1988) 1125–1133. doi:https://doi.org/10.1295/polymj.20.1125.

[28] P. Shrinivas, S. Kasapis, T. Tongdang, Morphology and mechanical properties of bicontinuous gels of agarose and gelatin and the effect of added lipid phase, Langmuir. 25 (2009) 8763–8773. doi:10.1021/la9002127.

[29] D. Baines, R. Seal, Natural Food Additives, Ingredients and Flavourings, 1st ed., Woodhead Publishing, 2012.

[30] N. Somboon, T.T. Karrila, T. Kaewmanee, S.J. Karrila, Properties of gels from mixed agar and fish gelatin, Int. Food Res. J. 21 (2014) 485–492.

[31] J. Wei, J. Wang, S. Su, S. Wang, J. Qiu, Z. Zhang, G. Christopher, F. Ning, W. Cong, 3D printing of an extremely tough hydrogel, RSC Adv. 5 (2015) 81324–81329. doi:10.1039/c5ra16362e.

[32] K. Nakamura, K. Harada, Y. Tanaka, Viscoelastic properties of aqueous gellan solutions: the effects of concentration on gelation, Top. Catal. 7 (1993) 435–447. doi:10.1016/S0268-005X(09)80239-7.

[33] S.R. Derkach, S.O. Ilyin, A.A. Maklakova, V.G. Kulichikhin, A.Y. Malkin, The rheology of gelatin hydrogels modified by κ-carrageenan, LWT - Food Sci. Technol. 63 (2015) 612–619. doi:10.1016/j.lwt.2015.03.024.

[34] A.H. Clark, R.K. Richardson, S.B. Ross-Murphy, J.M. Stubbs, Structural and Mechanical Properties of Agar/Gelatin Co-gels. Small-Deformation Studies, Macromolecules. 16 (1983) 1367–1374. doi:10.1021/ma00242a019.

[35] B.G. Compton, J.A. Lewis, 3D-printing of lightweight cellular composites, Adv. Mater. 26 (2014) 5930–5935. doi:10.1002/adma.201401804.

[36] R. Landers, U. Hübner, R. Schmelzeisen, R. Mülhaupt, Rapid prototyping of scaffolds derived from thermoreversible hydrogels and tailored for applications in tissue engineering, Biomaterials. 23 (2002) 4437–4447. doi:10.1016/S0142-9612(02)00139-4.

[37] Simplify3D, Print Quality Troubleshooting Guide, (2018). https://www.simplify3d.com/ (accessed June 8, 2020).

[38] Z. Liu, B. Bhandari, S. Prakash, S. Mantihal, M. Zhang, Linking rheology and printability of a multicomponent gel system of carrageenan-xanthan-starch in extrusion based additive manufacturing, Food Hydrocoll. 87 (2019) 413–424. doi:10.1016/j.foodhyd.2018.08.026.

[39] M.H. Lau, J. Tang, A.T. Paulson, Texture profile and turbidity of gellan/gelatin mixed gels, Food Res. Int. 33 (2000) 665–671. doi:10.1016/S0963-9969(00)00111-3.

[40] S. Banerjee, S. Bhattacharya, Compressive textural attributes, opacity and syneresis of gels prepared from gellan, agar and their mixtures, J. Food Eng. 102 (2011) 287–292. doi:10.1016/j.jfoodeng.2010.08.025.

[41] B.N. Turner, R. Strong, S.A. Gold, A review of melt extrusion additive manufacturing processes: I. Process design and modeling, Rapid Prototyp. J. 20 (2014) 192–204. doi:10.1108/RPJ-01-2013-0012.

[42] C. Le Tohic, J.J. O'Sullivan, K.P. Drapala, V. Chartrin, T. Chan, A.P. Morrison, J.P. Kerry, A.L. Kelly, Effect of 3D printing on the structure and textural properties of processed cheese, J. Food Eng. 220 (2018) 56–64. doi:10.1016/j.jfoodeng.2017.02.003.

[43] A.K. Sood, R.K. Ohdar, S.S. Mahapatra, Parametric appraisal of mechanical property of fused deposition modelling processed parts, Mater. Des. 31 (2010) 287–295. doi:10.1016/j.matdes.2009.06.016.